

Surface-plasmon coupling in cylindrical pores

M. Schmeits

Institut de Physique, Université de Liège, B-4000 Sart Tilman (Liège) 1, Belgium

(Received 5 December 1988)

We have determined the surface-plasmon modes of cylindrical pores in metals and of pairs of coupled cylindrical pores having parallel axes. The eigenfrequencies and the polarization fields are determined in the case of interacting pores of equal radii where the modes are even or odd with respect to the symmetry plane. Numerical application is made for pores in aluminum with inner radii of 20 Å and separation of the axes of 48 Å. The surface-plasmon frequencies and the polarization fields show strong differences with respect to the case of an isolated pore. Frequency shifts up to 2 eV occur, leading in particular to the appearance of two new modes at energies well below the flat-surface-plasmon frequency $\omega_p/\sqrt{2}$. For the one- and two-cylindrical-pore configurations, we have established an expression for the second-quantized interaction Hamiltonian between an electron and the surface-plasmon modes, from which the energy-loss probability for an electron moving parallel to the cylindrical axis is obtained. Application to the scattering of electrons of 10 keV kinetic energy shows, for both configurations, substantial differences in the energy-loss spectra as compared to the flat-surface case. In addition, the loss function for the pair of cylindrical pores is strongly affected by the coupling of the surface-plasmon fields of the two interacting pores.

INTRODUCTION

Initiated by the pioneering work of Ritchie¹ in 1957, surface plasmons have been the subject of intense theoretical and experimental investigations during the past few decades. The existence of surfaces leads to the creation of new modes which are absent in the bulk. Surface-plasmon modes have eigenfrequencies and polarization fields which are dependent on the geometrical shape of the surface. Flat surfaces, thin films, and spherical-shaped surfaces have extensively been studied.^{2,3} In particular, fast-electron spectroscopy has been a powerful tool in the investigations on the properties of these surface collective excitations. A charged particle moving close to the surface of a polarizable body interacts with the electromagnetic field of the surface modes and suffers characteristic losses at energy values which are integer multiples of the quantized surface-plasmon energies. The energy position and the strength of the energy-loss peaks for a given electron trajectory provide information on the characteristic eigenmodes of the solid and on the interaction mechanism between the electron and these eigenmodes.

Reflection experiments with flat surfaces or transmission experiments with thin films have been made since the early 1960s. Scattering by spherical particles has been performed only recently by Batson and Treacy,⁴ using scanning transmission electron microscopy (STEM). The present achievements of this technique allow one to produce electron beams whose width is less than 1 nm. Batson and Treacy studied the losses of fast electrons on oxide-covered aluminum particles of typically 10 nm radius. When modifying the position of the electron beam with respect to the center of the sphere, it is possible to choose electron trajectories where the electron crosses the metal, or whether it remains outside, leading to

energy-loss features strongly dependent on the value of the impact parameter.

The first part of this paper is devoted to a theoretical study of the inelastic scattering of fast electrons by surface plasmons on cylindrical pores. The aim is to obtain the energy-loss probability as a function of the parameters describing the cylindrical pore and the electron trajectory, namely, the pore radius, the substrate plasmon frequency ω_p , the kinetic energy of the electron, and the distance of the electron path with respect to the pore wall. The first experimental investigation of electron scattering by cylindrical pores was reported by Warmack *et al.*⁵ The target consisted of silver metallic foils perforated by microchannels of radius of 20–200 nm. The channels were uniformly illuminated by the electron beam. Microchannels of much lower size seem, however, to be possible, making the losses more sensitive to the pore curvature. Warmack *et al.* observed that the passage of electrons results in energy-loss structures, which they attributed to the excitation of surface plasmons. Unfortunately, the experimental procedure did not allow one to obtain a detailed dependence of the energy-loss function on the electron trajectory, as the beam width was larger than the pore diameter. In a later paper, Mamola *et al.*⁶ reported energy-loss experiments by a microchannel array. They interpreted the disagreement of their experimental result with energy losses calculated for electrons moving parallel to flat surfaces (an approximation valid for the range of pore radii used) in terms of excitation of localized surface plasmons on roughness structures close to the ends of the microchannels.

An alternative explanation could be that the coupling of surface plasmons on neighboring channels is at least partly responsible for the modification of the surface-plasmon energies and henceforth for the shape of the energy-loss function. In the second part of this paper, we

study the surface-plasmon modes of a pair of coupled cylindrical pores and determine the energy-loss function for an electron transmitted through one of the cylindrical channels. That the coupling between neighboring cylindrical pores may be important is suggested by the experiment of Batson on a system having similar properties.^{7,8} He studied the inelastic-scattering process of fast electrons on clusters of 10–50-nm-diam aluminum spheres. For certain electron trajectories he observed energy losses between 2.5 and 4.0 eV, i.e., at values completely split off from the 6.3-eV surface-plasmon energy of an isolated sphere. He attributed these losses to the excitation of a bispherical plasmon mode, as was consistent with the peak position and the spatial variation of the scattering probability.

The theoretical methodology that will be used for both the one- and two-cylinder systems is based on a formalism which was first applied by Lucas *et al.*⁹ for the thin-film case and which has been successful in explaining the energy losses of fast electrons by oxide-covered metallic particles.^{10,11} First, we determine the surface-plasmon frequencies by solving Laplace's equation in the nonretarded limit. In the study of the inelastic-electron-scattering process, the electron is described classically as a sink or a source of energy, an approximation which is valid at sufficiently high electron energies. In the next step, we establish a Hamiltonian formalism to describe the free-polarization eigenmodes of the cylindrical pore systems and their coupling to the fast charged particle. Finally, we obtain the energy-loss probability for given cylindrical radii and interdistance and for a fixed electron trajectory.

Numerical application of our results is made to isolated cylindrical pores of inner radius $a = 20 \text{ \AA}$ and to pairs of parallel cylindrical pores of the same radius, their axes being separated by 48 \AA . For both configurations, we will show that the curvature effect is important in giving rise to energy-loss features different from those encountered in flat-surface scattering. In the case of a pair of cylindrical pores, we will show that the coupling of the surface plasmons leads to new plasmon modes having eigenfrequencies and polarization fields which are different from those of the isolated cylinders. This will strongly influence the energy-loss probability for an electron moving parallel to the common cylindrical axis.

I. CYLINDRICAL PORE

A. Surface-plasmon modes

We first study the plasmon modes in a metal containing a cylindrical pore of constant section and infinite length. The inner radius of the pore will be labeled a . The metal is described by a Drude-like dielectric function

$$\epsilon(\omega) = 1 - \omega_p^2 / \omega^2. \quad (1)$$

Inside the pore the dielectric constant ϵ_0 is taken equal to 1, as corresponds to vacuum.

In order to determine, in the nonretarded limit, the surface-plasmon frequencies of a cylindrical pore, Laplace's equation is solved in the two regions bounded

by the cylindrical wall and the electrical potential and normal component of the displacement vector are matched at the interface.

In cylindrical coordinates, the solutions of Laplace's equation, which have to be finite everywhere, can be written

$$\varphi_{mk}^{(1)}(\mathbf{r}) = A_{mk} \frac{I_m(k\rho)}{I_m(ka)} e^{im\theta} e^{ikz} \quad \text{for } \rho < a \quad (2)$$

and

$$\varphi_{mk}^{(2)}(\mathbf{r}) = B_{mk} \frac{K_m(k\rho)}{K_m(ka)} e^{im\theta} e^{ikz} \quad \text{for } \rho > a, \quad (3)$$

where $I_m(k\rho)$ and $K_m(k\rho)$ are modified Bessel functions, and A_{mk} and B_{mk} are constants to be determined. The z axis is chosen along the cylindrical axis. The eigenmodes are therefore classified by a continuous index k and a discrete index m . Expressing the continuity of the electrical potential at $\rho = a$, one obtains

$$A_{mk} = B_{mk}. \quad (4)$$

The continuity of the normal component of the displacement vector yields the allowed values of the dielectric function

$$\epsilon_{mk} = \frac{I'_m(ka)K_m(ka)}{I_m(ka)K'_m(ka)}. \quad (5)$$

The prime means derivation with respect to the argument. The resulting eigenfrequencies for the cylindrical-pore-plasmon modes are then

$$\omega_{mk} = \omega_p [-ka I'_m(ka) K'_m(ka)]^{1/2}. \quad (6)$$

For comparison, we mention the expression of the eigenfrequencies for the cylindrical fiber, i.e., the system where $\epsilon(\omega)$ and ϵ_0 have been interchanged with respect to the cylindrical pore case. They are given by

$$\omega_{mk} = \omega_p [ka I'_m(ka) K_m(ka)]^{1/2}. \quad (7)$$

In Fig. 1 we show the dispersion relations for both the cylindrical pore and the cylindrical fiber, for the five lowest values of m . All cylindrical-pore-plasmon frequencies are greater or equal to the flat-surface-plasmon frequency $\omega_p / \sqrt{2}$, whereas the full-cylinder-plasmon frequencies are lower or equal to $\omega_p / \sqrt{2}$. A similar situation is found in spherical geometry. The eigenmodes for the spherical cavity are given by

$$\omega_l = \omega_p \left[\frac{l+1}{2l+1} \right]^{1/2}, \quad l = 0, 1, 2, \dots \quad (8)$$

Hence they are larger than $\omega / \sqrt{2}$. The eigenmodes of the spherical particle are

$$\omega_l = \omega_p \left[\frac{l}{2l+1} \right]^{1/2}, \quad l = 1, 2, 3, \dots \quad (9)$$

They are lower than $\omega_p / \sqrt{2}$.

Going back to the cylindrical-pore configuration, the limiting values for $ka \gg 1$ are $\omega_p / \sqrt{2}$, for all values of m .

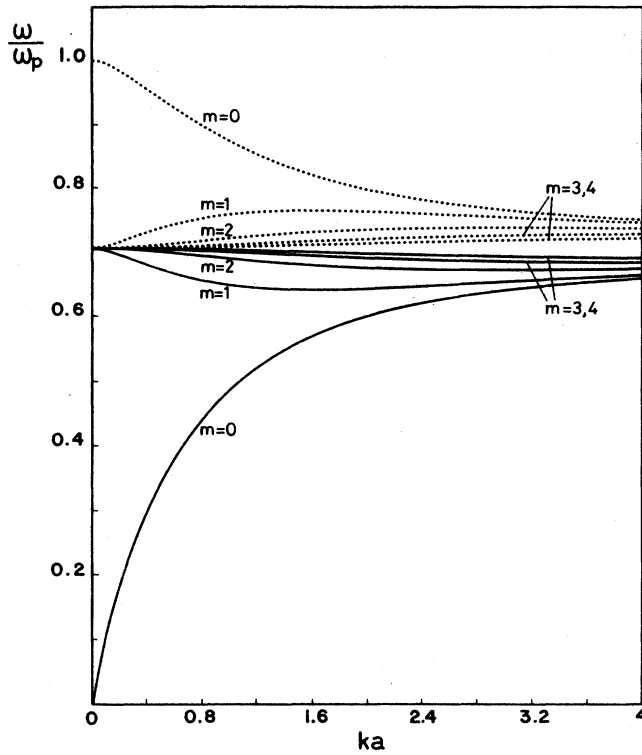


FIG. 1. Dispersion relations for surface-plasmon modes of a cylindrical pore (dotted lines) and for a cylindrical fiber (solid lines).

For large values of k , i.e., small plasmon wavelengths, the eigenfrequencies are not sensitive to the surface curvature. For $ka \ll 1$, i.e., the long-wavelength limit, the limiting values are $\omega_{mk} = \omega_p / \sqrt{2}$ for $m \neq 0$ and $\omega_{mk} = \omega_p$ for $m = 0$. This latter plasmon mode corresponds to an oscillation of the electronic charge with respect to the positive background having the same symmetry as the cylindrical surface. Its eigenfrequency is equal to the bulk-plasmon frequency ω_p , as is also the case for the $l=0$ breathing mode of the spherical void.

The electrical potential corresponding to each plasmon mode, as given by Eqs. (2) and (3), is defined up to a normalization constant A_{mk} . The associated polarization modes are given by

$$\mathbf{P}_{mk}(\mathbf{r}) = \frac{1 - \epsilon_{mk}}{4\pi} \nabla \varphi_{mk}(\mathbf{r}). \quad (10)$$

In the following, the normalization constant A_{mk} is chosen such that the polarization modes are orthonormal,

$$\int d\mathbf{r} \mathbf{P}_{m'k'}^*(\mathbf{r}) \cdot \mathbf{P}_{mk}(\mathbf{r}) = \delta_{m,m'} \delta(k - k'). \quad (11)$$

This yields the following value for A_{mk} :

$$A_{mk} = 2[-kaK_m(ka)K'_m(ka)]^{1/2}. \quad (12)$$

B. Electron-surface-plasmon interaction Hamiltonian

In the next step, a second-quantization description of the surface-plasmon field is introduced, using a methodology similar to that which has been applied to flat surfaces, thin films, or spherical-shaped surfaces.³ In terms of surface-plasmon creation and annihilation operators a_{mk}^\dagger and a_{mk} , the total surface-plasmon Hamiltonian can be cast into the harmonic-oscillator form,

$$H_0 = \sum_{m,k} \hbar \omega_{mk} (a_{mk}^\dagger a_{mk} + \frac{1}{2}). \quad (13)$$

The total electrical potential can be expressed in terms of the same operators, leading to an expression of the interaction Hamiltonian H_I between an electron at a fixed position \mathbf{r} and the surface-plasmon field, linear in the creation and annihilation operators a_{mk}^\dagger and a_{mk} :

$$H_I(\mathbf{r}) = \sum_{m,k} h_{mk}(\mathbf{r}) (a_{mk}^\dagger + a_{mk}), \quad (14)$$

where

$$h_{mk}(\mathbf{r}) = e \left[\frac{\hbar \omega_p^2}{8\pi \omega_{mk}} \right]^{1/2} \varphi_{mk}(\mathbf{r}), \quad (15)$$

with $\varphi_{mk}(\mathbf{r})$ given by Eqs. (2), (3), and (12).

This is an analytical expression of the coupling functions depending on the cylindrical coordinates ρ , z , and θ . In particular, the z dependence is given by the exponential e^{ikz} term.

C. Loss function

An electron moving parallel to the cylindrical wall will interact with the surface-plasmon field and suffer energy losses equal to integer multiples of the quantized surface-plasmon energies $\hbar \omega_{mk}$. When the trajectory remains outside the metal, no bulk-plasmon modes will be excited, as the electrical field associated with the bulk modes is zero outside the metal. When part of the trajectory is going through the metal, bulk-plasmon losses will be observed in addition to the surface-plasmon losses. As we will discuss in the following only the contribution of the surface-plasmon losses, bulk effects will not be treated here.

The energy-loss function $P(\omega)$ is defined as the probability that at time $t = +\infty$ the plasmon system will be in a state of total energy $E = E_0 + \hbar \omega$ above the ground-state energy E_0 . It will be assumed that the electron is so fast that any momentum transfer occurring during the scattering process is much smaller than the electron momentum. This means that the kinetic energy of the electron remains essentially constant and that its trajectory suffers no displacements perpendicular to its initial velocity. In that approximation, the electron can be considered as a classical particle of constant velocity v and acts as a time-dependent perturbation on the surface-plasmon system.

The loss function $P(\omega)$ can then be obtained from the evolution of the surface-plasmon eigenstates,^{9,12} yielding, in general notations $i_i = (m, k)$,

$$P(\omega) = P_0 \sum_{n=0}^{\infty} \frac{\hbar^{-2n}}{n!} \times \sum_{i_1, \dots, i_n} |I_{i_1}|^2 \cdots |I_{i_n}|^2 \times \delta(\omega - (\omega_{i_1} + \omega_{i_2} + \cdots + \omega_{i_n})). \quad (16)$$

Here, I_{i_i} denotes the time-Fourier transform of the coupling function, i.e., for the cylindrical-pore system

$$I_{mk} = \int_{-\infty}^{+\infty} dt h_{mk}[\mathbf{r}(t)] e^{-i\omega_{mk}t}, \quad (17)$$

and P_0 is a normalization factor.

In expression (16), the $n=0$ term gives the no-loss probability, and the general n term of the series gives the strength of the energy loss due to multiple excitations of n eigenmodes, such that the total energy loss is equal to $\hbar\omega$. The energy-loss probability as given by expression (16) is normalized to unity.

For the following we will study energy losses suffered by an electron moving parallel to the cylindrical axis. Its trajectory in cylindrical coordinates is given by

$$\rho = \rho_e, \quad \theta = \theta_e, \quad z = vt. \quad (18)$$

The main energy losses will be due to one-plasmon excitations, the contribution of which in the sum (16) is given by

$$P_1(\omega) = \frac{P_0}{\hbar^2} \sum_{m,k} |I_{mk}|^2 \delta(\omega - \omega_{mk}). \quad (19)$$

For a cylinder of infinite length, the energy-loss probability would be infinite. Therefore, we have determined the (unnormalized) energy-loss probability per unit path length, denoted in the following by $Q_1(\omega)$ and which we define as follows: if the interaction h_{mk} is switched on during the interval $[-L/2, +L/2]$ and set equal to zero outside, the energy-loss function depends on the length L . The energy-loss probability per unit path length is then defined as the limiting value of

$$Q_1(\omega) = \lim_{L \rightarrow \infty} \left[\frac{1}{L} \frac{P_1(\omega, L)}{P_0} \right], \quad (20)$$

which has a finite value.

D. Electron scattering by a cylindrical pore

Application of the above expressions for the energy-loss probability $Q_1(\omega)$ in the case of an electron moving parallel to the axis of a cylindrical wall with $\rho_e < a$ yields, making use of the expressions (15), (17), (19), and (20),

$$Q_1(\omega) = \sum_{m,k} \frac{e^2 \omega_p^2}{\hbar v \omega_{mk}} [-kaK_m(ka)K'_m(ka)] I_m^2(k\rho_e) \times \delta(\omega_{mk} - kv) \delta(\omega - \omega_{mk}). \quad (21)$$

The energy loss depends on the electron trajectory through the factor $I_m^2(k\rho_e)$, and for the obvious reason of the cylindrical symmetry, it is independent of the polar

angle θ_e . For a trajectory such that $\rho_e > a$, the dependence would be proportional to $K_m^2(k\rho_e)$, as can be seen from the relations (3) and (15). The loss function $Q_1(\omega)$ is a sum of δ functions at values $\omega = \omega_{mk}$ such that $\omega_{mk} = kv$. This reduces the double sum over m and k to a single sum over m , such that for each m only one $k = k_m$ value is allowed, which corresponds to the intersection of the dispersion curve $\omega_m(k)$ with the line $\omega = kv$. The condition $\omega = \omega_{mk} = kv$ expresses that only those surface modes can be excited for which the phase velocity is equal to the electron velocity parallel to the surface. The same condition is encountered in the case of an electron moving parallel to a flat surface, or an electron reflected by a flat surface.^{13,14}

We have determined numerically the energy-loss probability, as given by expression (21) for the case of an electron having a kinetic energy of 10 keV, moving parallel to the walls of a cylindrical pore of inner radius $a = 20 \text{ \AA}$, at a distance $\rho_e = 17 \text{ \AA}$ from the cylindrical axis of a pore in an aluminum metal, for which we take $\hbar\omega_p = 15 \text{ eV}$. For ease of graphic presentation, we have replaced the different δ functions by Lorentzian functions of linewidth $\gamma = 0.5 \text{ eV}$. This simulates a damping factor in the classic dielectric function. In Fig. 2 we show the energy

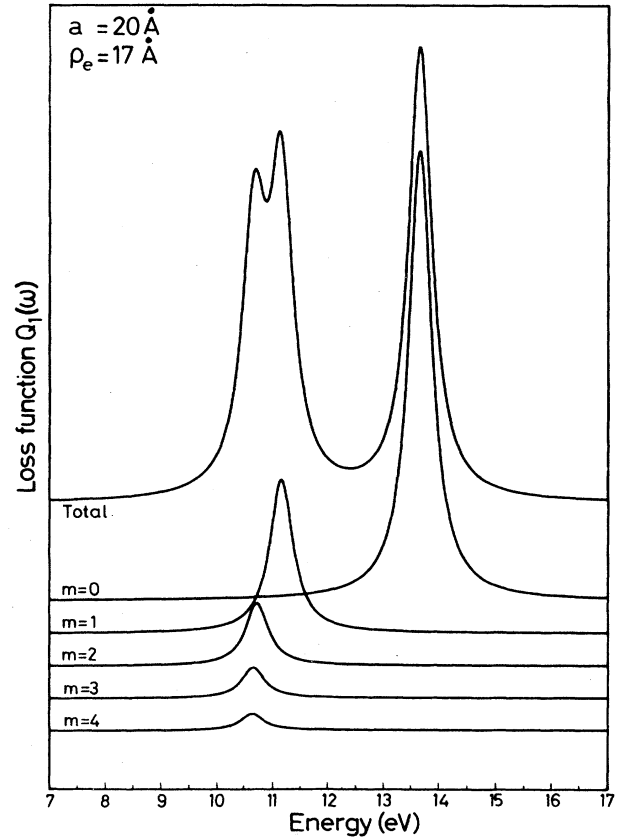


FIG. 2. One-plasmon energy-loss probability per unit path length for 10-keV electrons moving at a distance $\rho_e = 17 \text{ \AA}$ from the axis of a cylindrical pore of inner radius $a = 20 \text{ \AA}$, with bulk-plasmon frequency $\omega_p = 15 \text{ eV}$. The five lowest curves are for the $m = 0, 1, 2, 3,$ and 4 modes; the upper curve is the total energy loss.

losses due to the five first m modes, together with the total energy loss, where the sum over m contains sufficient terms to achieve convergence.

For an electron moving parallel to a flat surface, one would obtain only a single energy-loss peak at the surface-plasmon frequency $\omega_p/\sqrt{2}$. In the case of a cylindrical pore, energy losses occur at different ω_{mk} frequencies (where $k=k_m$) and their strength decreases with increasing m value. Within the chosen graphical resolution, the highest loss peak at 13.6 eV clearly results from excitation of the $m=0$ mode. The peak at 11.1 eV results from the $m=+1$ and -1 modes, and the structure at 10.6 eV contains all the energy losses due to higher modes.

The detailed shape of the energy-loss function is strongly dependent on the choice of the parameters describing the scattering process. Reducing the value of ρ_e not only reduces the strength of the energy-loss probability through the $I_m^2(k\rho_e)$ factor in expression (21), but also increases the relative importance of the $m=0$ mode. In particular, for $\rho_e=0$ the $m=0$ term is the only term remaining in the sum. Increasing the kinetic energy of the electron would increase the slope of the $\omega=kv$ line. As a consequence, as one can see from Fig. 1, the $m=0$ energy-loss peak would move up in energy, but all the lower energy-loss peaks would coalesce at a position close to $\omega_p/\sqrt{2}$.

An alternative way to determine the energy-loss function is to use a classical description by deriving the energy-loss probability from the work done on the electron by the electrical field reflected by the metallic surface.¹⁵ This yields an energy-loss probability given by

$$P_{cl}(\omega) = \frac{e^2}{\hbar v^2} \sum_{m,k} \text{Im} \left[\frac{\epsilon - 1}{\epsilon - \epsilon_{mk}} \right] \times \frac{I_m^2(k\rho_e) K_m(ka)}{I_m(ka)} \delta(\omega - kv). \quad (22)$$

Choosing a Drude-like expression of the dielectric function $\epsilon(\omega)$ with an imaginary part containing a damping factor g , expression (22) reduces to (21) in the limit $g \rightarrow 0$.

II. COUPLED CYLINDRICAL PORES

As in some samples it may happen that two cylindrical pores are close to each other, and so one may ask to what extent the energy-loss function may be influenced by the presence of the second pore. To answer this question we will proceed along the same lines as for the single-pore case: After a detailed study of the coupled plasmon modes, we will establish the interaction Hamiltonian and deduce the energy-loss probability.

A. Surface-plasmon modes

To obtain the eigenfrequencies and the polarization waves of the coupled plasmon system, one has again to solve Laplace's equation with appropriate boundary conditions for the particular system which is formed by two

parallel cylindrical pores of inner radii a and b . The distance between the two axes will be labeled R , and the used coordinates are illustrated by Fig. 3. The two cylindrical walls delimit three regions in space; the inner region of each cylinder will have a dielectric constant $\epsilon_1 = \epsilon_2 = 1$, whereas the outer region is characterized by a dielectric function $\epsilon_3 = \epsilon(\omega)$, as given by expression (1). For this two-cylinder system the translational invariance along z persists, but the rotational invariance around the z axis, of course, is nonexistent. There is no coordinate system in which the Laplace equation is separable and which would describe the cylindrical walls as constant coordinate surfaces.

We therefore are forced to use a numerical procedure in order to obtain the plasmon modes of the coupled-cylinder system. The starting point is similar to that which has been used to obtain the van der Waals interaction between cylindrical fibers^{16,17} or between spherical particles or spherical voids.^{18,19}

Using the coordinates illustrated by Fig. 3, the eigen-solutions of Laplace's equation are labeled $\varphi_{pk}(\mathbf{r})$, where k is again a wave number along the z axis, and p is an index which will be defined below.

In the three regions, these solutions can be written as

$$\varphi_{pk}^{(1)}(\mathbf{r}) = \sum_m A_{mk} \frac{I_m(k\rho_1)}{I_m(ka)} e^{im\theta_1} e^{ikz} \quad \text{if } \rho_1 < a, \quad (23)$$

$$\varphi_{pk}^{(2)}(\mathbf{r}) = \sum_m D_{mk} \frac{I_m(k\rho_2)}{I_m(kb)} e^{im\theta_2} e^{ikz} \quad \text{if } \rho_2 < b, \quad (24)$$

$$\varphi_{pk}^{(3)}(\mathbf{r}) = \left[\sum_m B_{mk} \frac{K_m(k\rho_1)}{K_m(ka)} e^{im\theta_1} + \sum_m C_{mk} \frac{K_m(k\rho_2)}{K_m(kb)} e^{im\theta_2} \right] e^{ikz} \quad \text{if } \rho_1 > a \text{ and } \rho_2 > b. \quad (25)$$

In order to apply the boundary conditions at the surface of the first cylinder, at $\rho_1 = a$, it is useful to express the term depending on ρ_2 and θ_2 in the outer potential in terms of ρ_1 and θ_1 , using an addition theorem for modified Bessel functions:²⁰

$$K_m(k\rho_2) e^{im\theta_2} = \sum_{j=-\infty}^{+\infty} K_{m+j}(kR) I_j(k\rho_1) e^{ij\theta_1}. \quad (26)$$

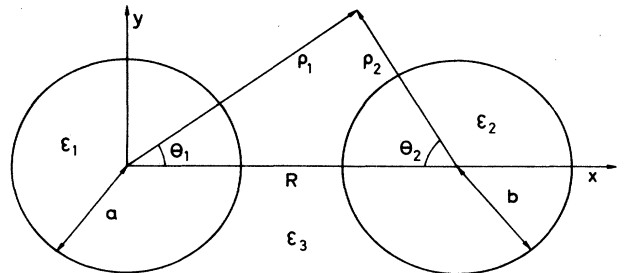


FIG. 3. Definition of the coordinates for the two cylinders of inner radius a and b , the axis-to-axis separation being R .

The continuity of the electrical potential at $\rho_1 = a$ yields

$$A_{mk} = B_{mk} + \sum_n \frac{K_{n+m}(kR)I_m(ka)}{K_n(kb)} C_{nk}, \quad (27)$$

which we can write in matrix form,

$$\mathbf{A} = \mathbf{B} + \mathbf{P}\mathbf{C}, \quad (28)$$

where $\mathbf{A}, \mathbf{B}, \mathbf{C}$ are vectors whose components are A_{mk} , B_{mk} , and C_{mk} respectively. \mathbf{P} is a matrix whose elements are

$$P_{mn} = \frac{K_{m+n}(kR)I_m(ka)}{K_n(kb)}. \quad (29)$$

The continuity of the normal component of the displacement vector at $\rho_1 = a$ yields

$$A_{mk} \frac{I'_m(ka)}{I_m(ka)} = \epsilon \left[B_{mk} \frac{K'_m(ka)}{K_m(ka)} + \sum_n \frac{K_{n+m}(kR)I'_m(ka)}{K_n(kb)} C_{nk} \right]. \quad (30)$$

Eliminating A_{mk} between (27) and (30) yields a set of relations between the coefficients B_{mk} and C_{mk} which can be cast into the matrix form

$$\mathbf{B} = \mathbf{M}\mathbf{C}, \quad (31)$$

where the matrix \mathbf{M} has the elements

$$M_{mn} = \frac{(\epsilon - 1)I'_m(ka)I_m(ka)K_m(ka)K_{m+n}(kR)}{[I'_m(ka)K_m(ka) - \epsilon I_m(ka)K'_m(ka)]K_n(kb)}. \quad (32)$$

In an analogous way, one can express the continuity relations at the surface of the second cylinder, obtaining vector relations

$$\mathbf{D} = \mathbf{Q}\mathbf{B} + \mathbf{C} \quad (33)$$

and

$$\mathbf{C} = \mathbf{N}\mathbf{B}, \quad (34)$$

where the matrices \mathbf{Q} and \mathbf{N} are obtained from \mathbf{P} and \mathbf{M} through permutation of the radii a and b .

From relations (31) and (34), one obtains

$$(\mathbf{M}\mathbf{N} - \mathbf{1})\mathbf{B} = \mathbf{0}. \quad (35)$$

The dispersion relations for the surface-plasmon modes are obtained by equating the determinant of this set of equations to 0,

$$\det(\mathbf{M}\mathbf{N} - \mathbf{1}) = 0. \quad (36)$$

If the two cylindrical pores have equal radii, then $\mathbf{M} = \mathbf{N}$ and $\mathbf{P} = \mathbf{Q}$, and Eq. (36) subdivides into two sets corresponding to

$$\det(\mathbf{M} + \mathbf{1}) = 0 \quad (37)$$

and

$$\det(\mathbf{M} - \mathbf{1}) = 0. \quad (38)$$

As will be seen below, the minus sign corresponds to modes which are symmetrical with respect to the plane $x = R/2$, and the plus sign corresponds to modes which are antisymmetrical with respect to this plane.

The problem which arises now is to find the plasmon modes from Eqs. (37) and (38), where the matrices are of infinite dimension. In Refs. 16 and 17 a series expansion valid in the thin-cylinder approximation (i.e., $R \gg a, b$) has been performed in order to obtain the leading terms in the van der Waals interaction energy. Such a development, however, is not valid for any distance R .

The numerical approach we have chosen, is to retain for each interacting cylinder only the modes for which $|m|$ is lower than a cutoff value m_{sup} . This limits the matrices $\mathbf{M} + \mathbf{1}$ and $\mathbf{M} - \mathbf{1}$ to the dimension $2m_{\text{sup}} + 1$, leading to a total number of modes equal to

$$N_d = 2(2m_{\text{sup}} + 1). \quad (39)$$

In each case convergence tests have been made with increasing values of m_{sup} in order to obtain convergence for the surface-plasmon modes, the polarization fields, and the surface-plasmon losses, for which results are presented here. The matrix elements M_{mn} are decreasing functions of the indices and the needed computational effort depends only on the required precision. Of course, the closer the distance R between the two cylinders, the larger the number of separate cylindrical modes which have to be retained.

In Figs. 4 and 5 we present the dispersion relations we have determined for the case of two parallel cylinders of equal radius $a = 20 \text{ \AA}$ and whose axes are separated by 48 \AA , i.e., 2.4 times the inner radius. In each figure we have shown only five of the pair modes, together with the

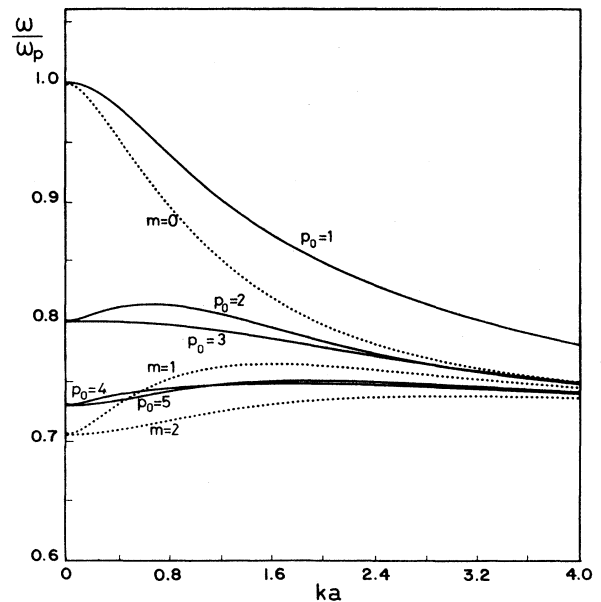


FIG. 4. Dispersion relations for the odd surface-plasmon modes of the two-cylindrical-pore system (solid lines). For comparison, the dispersion relations for the $m = 0, 1, 2$ isolated-cylinder-plasmon modes (dotted lines) are shown.

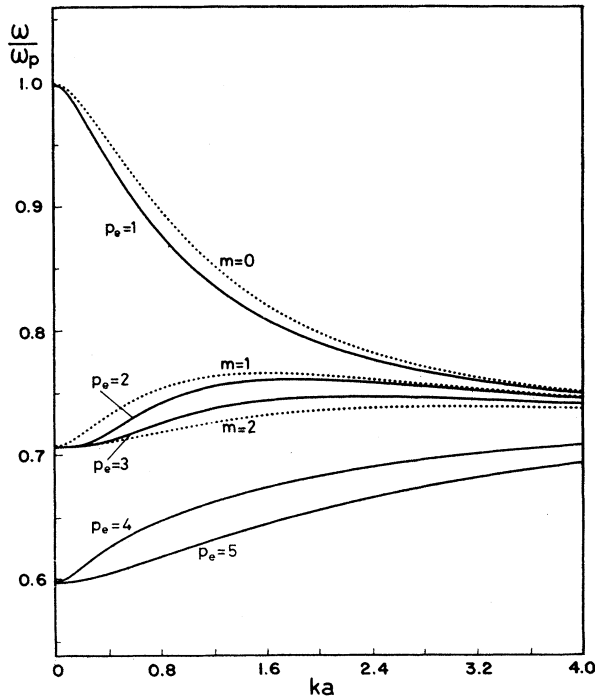


FIG. 5. Dispersion relations for the even surface-plasmon modes of the coupled-cylindrical-pore system (solid lines) and dispersion relations for the $m = 0, 1, 2$ isolated-cylinder-plasmon modes (dotted lines).

$m = 0, 1,$ and 2 isolated cylinder dispersion relations. Calculations have effectively been made with N_d , as defined by relation (39), equal to 22. The five modes which are shown here are those which reduce, when increasing the separation between the two cylinders, to the one-cylinder $m = 0, +1,$ and $+2$ modes. The other modes, not shown here, have energies between the lowest odd pair modes shown in Fig. 4 and $\omega_p/\sqrt{2}$. The pair modes which are shown in Fig. 4, solutions of Eq. (37), are odd with respect to the symmetry plane $x = R/2$ and have been labeled $p_o = 1, 2, \dots, 5$. This indexing is purely arbitrary. The even modes in Fig. 5 have been labeled p_e .

As one can see from Figs. 4 and 5, for the system under study there is a substantial modification of the dispersion-relation structure. Applied to an aluminum substrate, for which $\hbar\omega_p = 15$ eV, shifts up to 2 eV occur for low values of k . All odd pair modes move up in energy with respect to the modes from which they originate. Adding higher m terms to the determinantal equation produces each time an additional upward shift. For the even modes, the situation is different. The two modes $p_e = 4$ and 5 move downward in energy to frequencies substantially lower than the flat surface-plasmon frequency $\omega_p/\sqrt{2}$. All other modes remain above $\omega_p/\sqrt{2}$.

The one-cylinder mode $m = 0$ interacts with all other modes in such a way that each pair mode contains a partial contribution from it, but the two modes having the strongest $m = 0$ wave character are the two highest pair modes, namely, $p_e = 1$ and $p_o = 1$. A remarkable fact is

that for these two modes the $k = 0$ frequency does not shift with respect to the one-cylinder case and remains equal to the bulk-plasmon frequency ω_p . This particular property also exists for the plasmon modes of a system of two spherical cavities. All modes, as given by (8), shift when the voids approach each other, except for the breathing monopole $l = 0$ mode.¹⁸

Once the plasmon frequencies are known, it is possible to obtain for each eigenfrequency the corresponding electrical potential as expressed by Eqs. (23)–(25); the coefficients $A_{mk}, B_{mk}, C_{mk},$ and D_{mk} are obtained from (29), (31), (34), plus an additional normalization condition, which we have taken identical to that for the one-cylinder problem, requiring the different polarization modes to be orthonormal.

B. Electron-surface-plasmon interaction Hamiltonian

The second-quantization operators a_{pk}^\dagger and a_{pk} are introduced along the same lines as for the one-cylinder case, leading to an expression of the coupling functions $h_{pk}(\mathbf{r})$ given by relation (14), the electrical potential being obtained as expressed above. As a numerical procedure is required for solving the whole set of equations, analytical expressions are no longer possible. In Figs. 6–8 we show, for the 10 pair modes illustrated by Figs. 4 and 5, and at a particular value $k = 0.6/a$, the position dependence of the coupling function $h_{pk}(\mathbf{r})$.

In Fig. 6 we show the coupling functions $h_{pk}(\mathbf{r})$ for electron positions along the Ox direction, i.e., the direction joining the centers of the two cylinders. For all modes the coupling functions are real, and as the pair modes are either odd or even with respects to the x - z

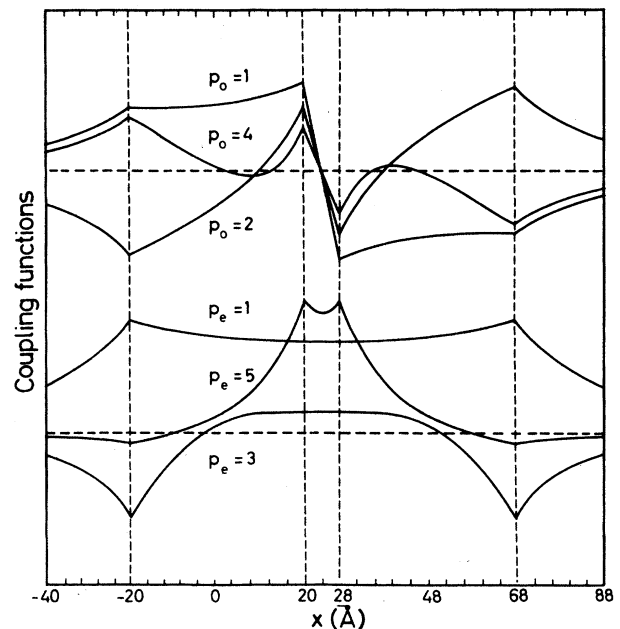


FIG. 6. Coupling functions $h_{pk}(\mathbf{r})$ for the even pair modes p_e and the odd pair modes p_o for r values along the x direction, joining the cylindrical axis, for $a = 20$ Å and $R = 48$ Å. The imaginary part is zero. Wave vector k is taken equal to $0.6/a$.

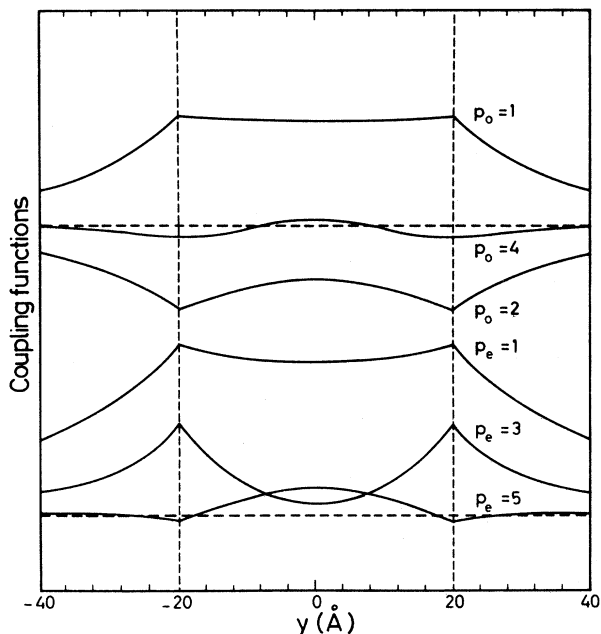


FIG. 7. Real part of the coupling functions $h_{pk}(\mathbf{r})$ for the even pair modes p_e and the odd pair modes p_o , for \mathbf{r} values along the y direction, for $a = 20 \text{ \AA}$, $R = 48 \text{ \AA}$, and $ka = 0.6$.

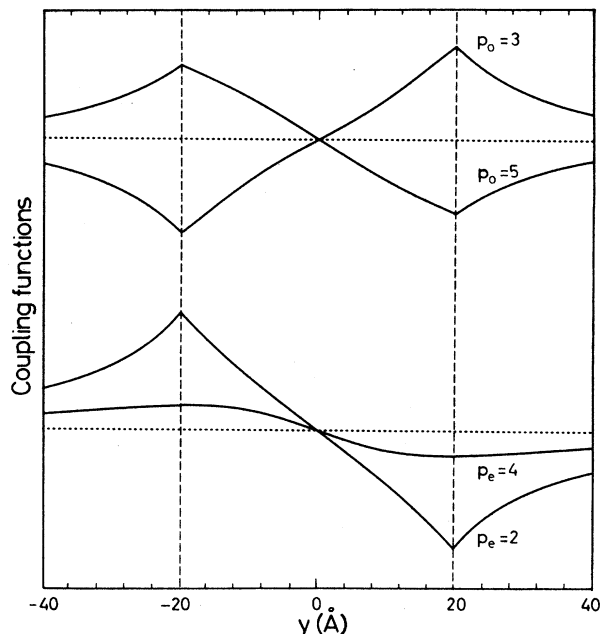


FIG. 8. Imaginary part of the coupling function $h_{pk}(\mathbf{r})$ for \mathbf{r} values along the y direction for $a = 20 \text{ \AA}$, $R = 48 \text{ \AA}$, and $ka = 0.6$.

plane, some of them have also their real part equal to zero. Therefore only the coupling functions corresponding to the even $p_e = 1, 3, 5$ modes and the odd $p_o = 1, 2, 4$ are shown, the other four being zero for \mathbf{r} on the x axis. As a general result, for the chosen two-cylinder system the interaction between the individual modes is so strong that the original potential symmetries have completely been lost. The modes $p_e = 1$ and $p_o = 1$, for example, have completely lost the minimum at the center of the cylinder which they had when at infinite separation.

The new character of the modes leads in some cases to coupling functions which are zero even for electron positions not on symmetry planes. See, e.g., $p_o = 4$ and $p_e = 5$. The behavior of the even $p_e = 5$ mode, in particular, is interesting. It is the mode which peels off from the mode continuum and has the lowest plasmon frequency. Its corresponding coupling function has the strongest amplitude of all the modes in the interspace between the two cylinders, but becomes very weak, even zero in some points, for x values such as $x < 0$, or $x > a + R$. This type of behavior will have important consequences for the dependence of the energy-loss function on the electron-beam position and, as will be seen below, is at the origin of the completely different energy-loss function in the paired-cylinder configuration, as compared to the isolated cylinder case.

In Figs. 7 and 8 we show the real and imaginary parts of the coupling functions for electron positions on the $0y$ axis, i.e., perpendicular to one of the cylindrical axes. For each mode either the real or imaginary part is equal to zero. These coupling functions will be useful in explaining the position dependence of the electron energy-loss probability.

C. Electron scattering by coupled cylinders

Starting from expressions (17)–(20), rewritten for the two-cylinder configuration, it is possible to obtain the energy-loss function per unit path length for an electron moving parallel to the z direction with a given trajectory described in cylindrical coordinates by a value of its radial position ρ_1 and of its polar angle θ_1 .

No analytic form of the energy-loss function is obtained, as already the pair-plasmon frequencies and the coupling functions are determined numerically. But, due to the e^{ikz} term in the coupling functions (24)–(26), there will again be a δ function $\delta(\omega_{pk} - kv)$ in the energy-loss probability, as in expression (21), and the corresponding one-plasmon energy-loss probability per unit path length is of the form

$$Q_1(\omega) = \sum_{p,k} |f_{pk}|^2 \delta(\omega_{pk} - kv) \delta(\omega - \omega_{pk}). \quad (40)$$

The factor $|f_{pk}|^2$ is essentially proportional to the square of the amplitude of the coupling functions (23)–(25).

We have determined the energy-loss function $Q_1(\omega)$ for a series of different positions of the electron beam with respect to the two-cylinder system. As for the one-cylinder case, we have, for a given electron velocity, determined numerically the modes which satisfy the surfing condition $\omega_{pk} = kv$, restricting the double sum in (40) to a single sum over p values. The energy-loss function reduces to a sum over discrete δ functions, which we have again replaced by Lorentzian functions as in the one-cylinder case.

In a first series of figures we show results for electron-scattering configurations for trajectories with equal

values of ρ_1 , i.e., equal distance of the beam with respect to the walls, but with different polar angle θ_1 . In the case of infinite separation of the pores, there would, of course, be no dependence on the polar angle θ_1 . In Figs. 9–11 we consider a 10-keV electron moving at a distance $\rho_1 = 17 \text{ \AA}$ from the axis of a cylinder of inner radius $a = 20 \text{ \AA}$, distant by 48 \AA from a second cylindrical pore of the same inner radius. The metallic substrate is characterized by a bulk-plasmon frequency $\hbar\omega_p = 15 \text{ eV}$.

In Fig. 9 we show for $\theta_1 = 0$ the total energy loss, as well as the contribution of the five even and odd modes for which we have previously shown the detailed dispersion relations and the coupling functions. As for the coupling functions, the partial energy loss of the modes $p_o = 3, 5$ and $p_e = 2, 4$ is not shown as it is equal to zero. A feature which has to be mentioned here is that in the total energy loss a double peak at 13.4 and 14.2 eV appears as due to the $p_e = 1$ and $p_o = 1$ modes, instead of the $m = 0$ peak at 13.65 eV in the one-cylinder energy-loss function shown in Fig. 2. The dominant peak in the energy-loss function results from the $p_e = 5$ mode. It is this peak, at an energy of 9.1 eV, which is well below the flat surface-plasmon frequency $\omega_p/\sqrt{2} = 10.6 \text{ eV}$, and even below all structures, that one observes in a scattering experiment on an isolated cylinder. The relative strength of this

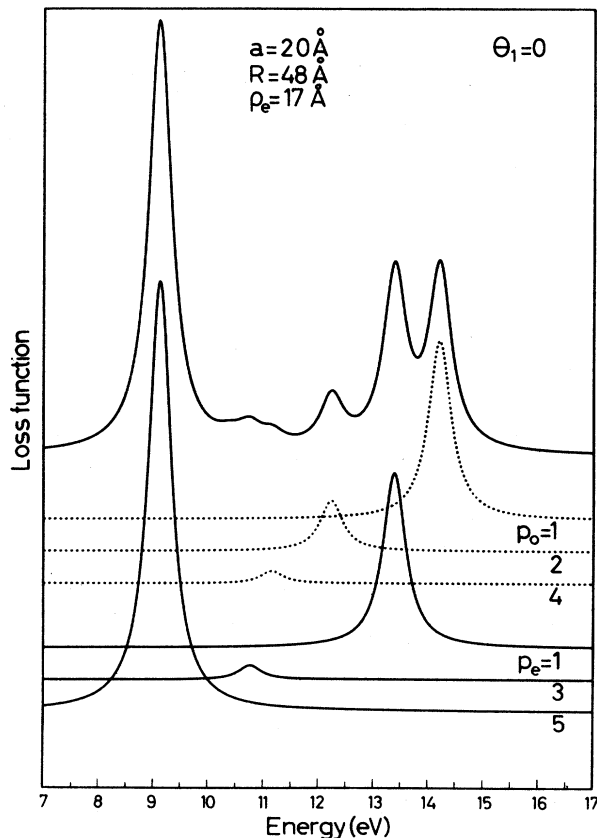


FIG. 9. One-plasmon loss function for the even (three lower curves) modes p_e and the odd modes p_o (dotted lines), together with total energy-loss function for an electron trajectory with $\rho_1 = 17 \text{ \AA}$ and $\theta_1 = 0$.

energy-loss peak is in relation with the amplitude of the coupling function of this mode, as illustrated in Fig. 6 for $ak = 0.6$. The losses due to the other modes (as well as those not shown here) are an order of magnitude lower.

In Fig. 10 we have shown the energy-loss functions for an electron trajectory with $\theta_1 = \pi/2$. As one can see, the total energy-loss spectra are completely different from the preceding ones. All pair-plasmon modes contribute to the energy-loss mechanism, even if for the $p_o = 4$ and $p_e = 5$ modes the energy loss is very small. The energy losses due to the two highest pair modes $p_o = 1$ and $p_e = 1$ are still well resolved, the energy losses due to the $p_o = 2$ and 4 modes lead to structures at 12.2 eV, and the contribution of all the other modes (including those not shown here) lead to a broad peak at 11 eV. The even $p_e = 4$ mode leads only to weak losses, and the ($p_e = 5$)-mode loss, which contributed to the dominant structure at $\theta_1 = 0$, has now completely disappeared. This results from the value of the coupling function at $\rho_1 = 17 \text{ \AA}$, $\theta_1 = \pi/2$, as is illustrated clearly by Fig. 7, showing that the coupling function, by accident, is changing its sign close to these parameter values.

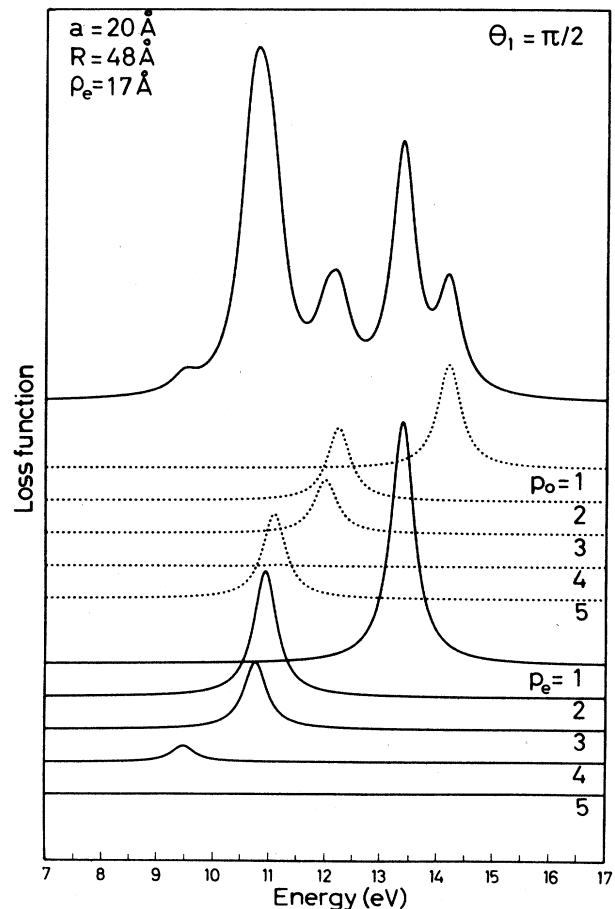


FIG. 10. One-plasmon energy-loss function for the even plasmon modes p_e and the odd plasmon modes p_o , together with the total energy-loss function for an electron trajectory with $\rho_1 = 17 \text{ \AA}$ and $\theta_1 = \pi/2$.

In Fig. 11 we show, for comparison, total energy-loss spectra corresponding respectively to values of $\theta_1=0$, $\pi/4$, $\pi/2$, $3\pi/4$, and π . It shows the evolution of the energy-loss spectra when moving the electron beam at a constant radial distance ρ_1 . The energy losses due to the low-frequency modes $p_e=4$ and 5 are observed only for the two spectra of $\theta_1=0$ and $\pi/4$, i.e., for electron trajectories crossing the region close to the second cylinder. Whereas the energy-loss functions for $\theta_1=0$ and π show strong differences, there is a close resemblance between the three upper curves, for $\theta_1=\pi/2$, $3\pi/4$, and π , i.e., for electron trajectories where the presence of the second cylinder is felt less strongly.

In Fig. 12 we show the energy-loss functions for five different electron trajectories, corresponding to $\theta_1=0$ or π , with x , respectively, equal to $R/2, 2a/3, 0, -2a/3, -R/2$. Again there is no symmetry in the energy-loss functions with respect to a cylindrical axis. Only those modes which are even with respect to the $x-z$ plane contribute to the energy-loss mechanism, namely those for which the coupling function has been shown in Fig. 6. The first spectra, for $x=R/2$, corre-

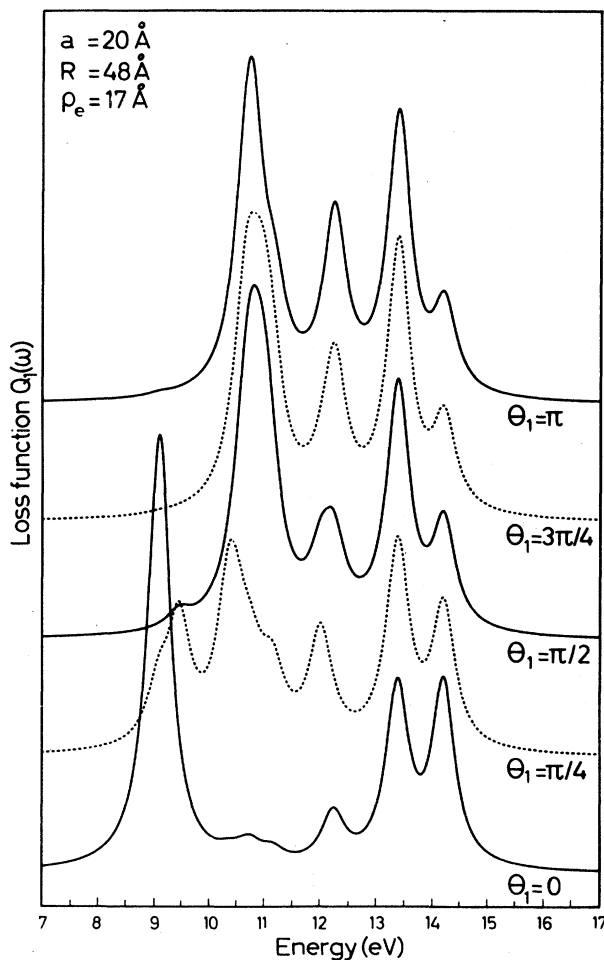


FIG. 11. Total one-plasmon energy-loss function for electron trajectories corresponding to $\rho_1=17 \text{ \AA}$ and $\theta_1=0, \pi/4, \pi/2, 3\pi/4$, and π .

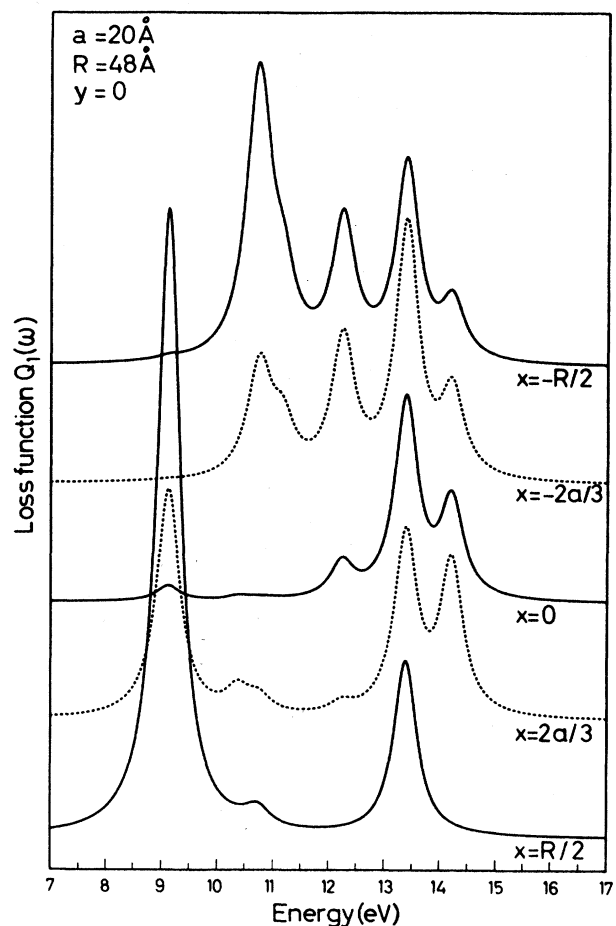


FIG. 12. Total one-plasmon energy-loss function for electron trajectories crossing the x axis with $x=R/2, 2/3a, 0, -2/3a$, and $-R/2$.

spond to a trajectory contained in the $x=R/2$ symmetry plane. Therefore, all odd p_o modes lead to zero energy losses; only the even modes contribute. As a result, only the three modes $p_e=1, 3, 5$ among those shown in Figs. 3 and 4 give rise to energy losses, which one retrieves in the peaks, respectively, at 13.4, 10.5 (together with other modes), and 9.1 eV. In particular, the odd $p_o=1$ mode has disappeared. For this configuration, the even $p_e=5$ peak has the strongest amplitude, as compared to other configurations.

If the electron beam is displaced towards decreasing x values, the odd modes again start to give rise to energy losses, as one can see from the reappearance of the odd $p_o=1$ loss at 14.2 eV. The even $p_e=5$ mode, in turn, is strongly decreasing in amplitude, which is again explained with the values of the coupling functions as shown in Fig. 6. The intensity of the energy losses are weakest at $x=0$, but it is worth mentioning that the spectrum is completely different from that one would have for an isolated cylinder, as, due to the contribution of only the $m=0$ mode, there would be a single peak at 13.6 eV. The two upper curves, in turn, show a four-peak structure which is essentially due to the modes shown in Fig. 6—except for $p_e=5$.

It should be noticed that the two spectra for $x = R/2$ and $-R/2$ correspond to electron trajectories across the metallic substrate. This implies that other inelastic energy-loss processes have been neglected, at least for this energy range. For example, bulk-plasmon losses at $\omega = \omega_p$ would occur and would be present in the energy-loss spectra, but without overlapping with most of the surface-plasmon structures. Inclusion of bulk-plasmon energy losses in our formulation would not present a fundamental difficulty.¹⁰

In comparing finally the energy-loss spectra of the two-cylinder system, with those of a single cylinder, as shown in Fig. 2, marked differences can be observed. The coupling of the cylinder modes leads to new plasmon frequencies and hence to new properties contained in the coupling functions, which completely modify the energy-loss spectra.

CONCLUSIONS

In the present paper we have studied the surface-plasmon modes of single cylindrical pores and of a pair of coupled parallel cylindrical pores. Using a Hamiltonian formalism we have determined the one-plasmon energy-loss probabilities for electron trajectories parallel to the cylindrical axis.

Application to cylindrical pores of 20-Å inner radius in an aluminum host metal and to pairs of pores such that the axes are separated by 48 Å show marked differences in the plasmon frequencies and in the energy-loss functions as compared to a flat-surface configuration. These differences result from the effect of the surface curvature

and the coupling between surface-plasmon modes on neighboring cylindrical pores. Among these new features appearing for the system of two coupled cylindrical pores, we mention a split by 1 eV for the $m = 0$ mode and the appearance of a completely new mode at 9 eV, i.e., at 1.5 eV below the surface-plasmon-mode bands of isolated cylinders. This mode leads to prominent energy losses for electron trajectories close to the interfacial region between the two cylindrical pores. Another important consequence of the coupling is the strong dependence of the energy-loss function on the cylindrical polar angle, in striking contrast to the situation for an isolated cylindrical pore.

Experimental observation of these features would require the use of scanning transmission electron microscopy, analogous to the technique used by Batson^{7,8} for studying energy losses by coupled spherical particles. Direct experimental comparison with our results would require microchannels of sizes and interdistances of the same order of magnitude as those used in the calculations. Their section should be circular and the inner wall sufficiently smooth such that roughness effects could be neglected. These constraints will be difficult to realize with the use of the presently available preparation technology.

Our work has shown that coupling effects are important and could be taken into account in the explanation of the observed experimental energy losses on microchannel arrays. For a detailed comparison, a study of cylindrical-pore arrays would be necessary, considering a superlattice of coupled cylindrical pores. This would yield bands of cylindrical modes instead of the pair modes we have labeled p_o or p_e .

¹R. H. Ritchie, *Phys. Rev.* **106**, 874 (1957).

²E. N. Economou and K. L. Ngai, *Adv. Chem. Phys.* **27**, 265 (1974).

³M. Schmeits and A. A. Lucas, *Progr. Surf. Sci.* **14**, 1 (1983).

⁴P. E. Batson and M. M. J. Treacy, in *Proceedings of the 38th Annual EMSA Meeting, San Francisco, 1980*, edited by G. W. Bailey (Claitors, Baton Rouge, LA, 1980).

⁵R. J. Warmack, R. S. Becker, V. E. Anderson, R. H. Ritchie, Y. T. Chu, J. Little, and T. L. Ferrel, *Phys. Rev. B* **29**, 4375 (1984).

⁶K. C. Mamola, R. J. Warmack, and T. L. Ferrell, *Phys. Rev. B* **35**, 2682 (1987).

⁷P. E. Batson, *Phys. Rev. Lett.* **49**, 936 (1982).

⁸P. E. Batson, *Ultramicrosc.* **9**, 277 (1982).

⁹A. A. Lucas, E. Kartheuser, and R. J. Badro, *Phys. Rev. B* **2**, 2488 (1970).

¹⁰S. Munnix and M. Schmeits, *Phys. Rev. B* **32**, 4192 (1985).

¹¹P. E. Batson, *Surf. Sci.* **156**, 720 (1985).

¹²A. A. Lucas and M. Šunjić, *Progr. Surf. Sci.* **2**, 75 (1972).

¹³A. Howie and R. H. Milne, *Ultramicrosc.* **18**, 427 (1985).

¹⁴A. Howie and R. H. Milne, *J. Microsc.* **136**, 279 (1984).

¹⁵M. Schmeits, *Solid State Commun.* **67**, 169 (1988).

¹⁶D. J. Mitchell, B. W. Ninham, and P. Richmond, *J. Theor. Biol.* **37**, 251 (1972).

¹⁷D. J. Mitchell, B. W. Ninham, and P. Richmond, *Biophys. J.* **13**, 359 (1978).

¹⁸A. A. Lucas, A. Ronveaux, M. Schmeits, and F. Delanaye, *Phys. Rev. B* **12**, 5372 (1975).

¹⁹R. Ruppin, *Phys. Rev. B* **26**, 3440 (1982).

²⁰D. Langbein, in *Theory of Van der Waals Attraction*, Vol. 72 of *Springer Tracts in Modern Physics*, edited by G. Höhler (Springer, Berlin, 1974), p. 57.